

Discovery of Sodium-Doped Triphenylene Superconductors by Searching the Organic Material Database

Taekyung Yoon,^{||} Ina Park,^{||} Thao Phuong Nguyen, Duck Young Kim, Jinho Lee, Ji Hoon Shim,^{*} and Hee Cheul Choi^{*}

HPSTAR
935-2020



Cite This: *Chem. Mater.* 2020, 32, 3358–3364



Read Online

ACCESS |



Metrics & More

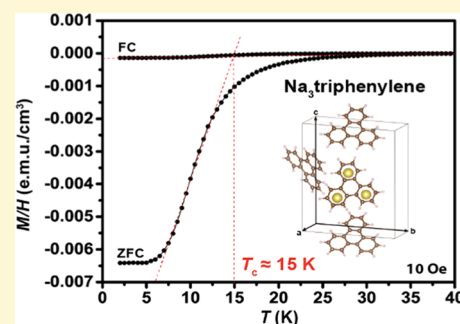


Article Recommendations



Supporting Information

ABSTRACT: Over the past few decades, there has been a lot of research on organic molecule-based materials for future advanced technology. The superconductivity has also been reported in various carbon-based organic materials in line with this trend. In particular, polycyclic aromatic hydrocarbons (PAHs) have been intensively studied in recent years because of the highly conjugated characteristics of the delocalized electrons supplied by alkali metal doping. Here, we report on a PAH superconductor, sodium-doped triphenylene (nominal composition of $\text{Na}_3\text{triphenylene}$), which was discovered by searching the database of PAH molecules with a small energy difference between the lowest unoccupied molecular orbital (LUMO) and LUMO + 1 states. As the first sodium-doped PAH superconductor, it shows the superconducting transition at $T_c \approx 15$ K under ambient pressure. The discovery of the new PAH superconductor suggests the promising possibility of superconductivity from more diverse molecular structures and the realization of high- T_c organic superconductors furthermore.



1. INTRODUCTION

After the first discovery of superconductivity in graphite intercalation compounds (GICs) in 1965,¹ carbon-based superconductors have received much attention, including carbon nanotubes^{2,3} and graphene.⁴ They possess a relatively low T_c value as a limitation in comparison to inorganic superconductors, such as copper (or iron)-based superconductors, for which T_c reaches 133 K in $\text{HgBa}_2\text{Ca}_2\text{Cu}_3\text{O}_8$ ⁵ and 56 K in $\text{Sr}_{0.5}\text{Sm}_{0.5}\text{FeAsF}$ ⁶ at ambient pressure. Nevertheless, they are still being studied intensively because of their low toxicity, abundant quantity, cheaper price, lighter weight, and mechanical flexibility, especially those that are important requirements for next-generation electronics. Development of carbon-based superconductors holds significance not only for extending to organic molecular materials from inorganic materials for high- T_c superconductors but also for studying their fundamental but veiled physical and chemical properties. One of the core categories of carbon-based materials is hydrocarbon molecules composed only of carbon and hydrogen atoms. In particular, polycyclic aromatic hydrocarbons (PAHs) made up of sp^2 carbons and fused benzene rings have attracted significant interest. Their extended π -bonding orbitals can delocalize the externally supplied electrons by alkali metal doping and can be the key factor to realize the metallic state. Although several PAH superconductors have been reported recently, the mechanism underlying the superconductivity has not yet been clearly understood because of their low reproducibility and a small magnetic shielding fraction, which are due to inhomogeneous

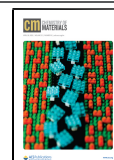
alkali metal vapor intercalation and the small size of crystallites. Thus, successful synthesis of new PAH superconductors with high reproducibility is very crucial in terms of securing the research on the high- T_c superconductivity of organic crystals.

The above-mentioned limitations in the synthesis of PAH superconductors make it difficult to explore and discover new PAH superconductors. In this study, we used the computational approach to explore the vast number of PAH molecules and find out the candidate molecules that have the possibility to show superconductivity. Since it has been reported that the small splitting between the lowest unoccupied molecular orbital (LUMO) and LUMO + 1 energy levels is a necessary condition for the multi-band Fermi liquid nature⁷ and possible superconducting phase, we used $\Delta = E_{\text{LUMO}+1} - E_{\text{LUMO}}$ as a key parameter to extract the superconducting candidate molecules. Among several candidates of PAH molecules with small Δ , we experimentally confirmed that sodium-doped triphenylene ($\text{Na}_3\text{triphenylene}$) shows superconductivity with $T_c \approx 15$ K. Note that sodium is first intercalated to synthesize a PAH superconductor by annealing after grinding molten sodium and the powder precursor directly. This work demonstrates the search for super-

Received: October 24, 2019

Revised: March 24, 2020

Published: March 24, 2020



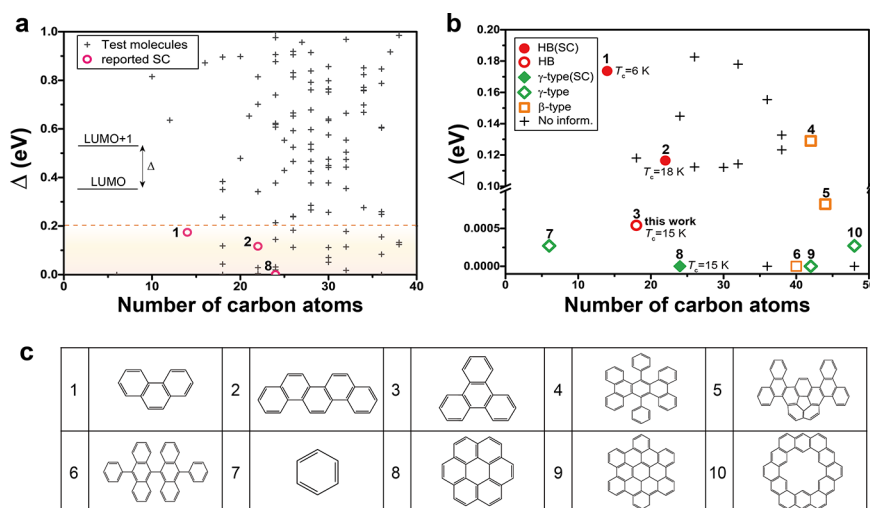


Figure 1. Calculation of Δ for 200 PAH molecules. Energy difference (Δ) versus the number of carbon atoms for (a) 200 PAH molecules (some points are located in the area outside the graph) and (b) the molecules corresponding to the area under the dashed line in (a) with markings representing the stacking type. (c) A table depicting the molecular structure of numbered molecules in (b).

conductivity in a highly symmetric and fully benzenoid molecular system, as well as in long-chain phenanthrene-edge-type molecules like picene⁸ and phenanthrene.⁹

2. METHODS

2.1. Triphenylene Purification and Preparation of Sodium-Doped Triphenylene. Triphenylene powder (98.0% purity, Sigma-Aldrich) was purified by the sublimation method and loaded at the end of a Pyrex glass tube (16 mm diameter, 300 mm length). The tube was connected to a center hole (12 mm diameter) perforated blank flange by a torr seal (Agilent technologies) to create a vacuum of up to 8.0×10^{-7} Torr. It was then placed at the center of a tubular furnace after vacuum sealing. The temperature increased up to 130 °C in 1 day and the tube was kept for 6 days at this temperature. An ampoule containing sodium (99.5% purity, Alfa Aesar) was heated to purify and melt the sodium using a hot plate. To prevent the oxidation of precursors, all sample preparation processes were carried out in a glovebox (with oxygen and moisture less than 0.5 ppm). A glass pipet (1 mm diameter) was fixed with a plastic syringe (1 mm volume) by a glue gun. The pipet was used to suck out the melted sodium metal and the unnecessary parts were cut out; thereafter sodium was injected into the Pyrex mortar on a heated hot plate at 240 °C.

Purified triphenylene was poured into the Pyrex mortar and directly ground with sodium to induce preintercalation of sodium into triphenylene for a specific time. Only short-time grinding is needed to avoid the loss of crystallinity (see the Supporting Information, Figure S1). The color of the sample changed from white to gray depending on the grinding time (see the Supporting Information, Figure S2). The ground sample was added to the Pyrex glass tube and annealed in the vacuum-sealed glass tube under 8.0×10^{-7} Torr for 20 h at 198 °C in an oven. The color of the doped samples was completely changed to black. The nonsuperconducting sodium-doped triphenylene was prepared (for unknown reasons) in the same way and confirmed by measurement of its magnetic properties.

2.2. Measurement of Magnetic Susceptibility of Sodium-Doped Triphenylene. The magnetic properties of sodium-doped triphenylene were measured by a SQUID MPMS (MPMS XL-7, Quantum Design). A gelatin capsule (AGC1, Quantum Design) filled with doped black powder crystals was fixed using clear plastic straws (AGC2, Quantum Design) to measure the magnetic susceptibilities.

2.3. Heat Capacity Measurement. Sodium-doped triphenylene was mixed with pure copper powder (99.999% purity, Sigma-Aldrich), and then made into a pellet (CuTPH in this text) using a hand press to maintain its form for measurement. The heat capacity of CuTPH was measured by PPMS (DynaCool, Quantum Design) after the

measurement of grease (N grease, Apiezon), which can facilitate heat conduction. All processes except measurements were carried out in the glovebox (with oxygen and moisture less than 0.1 ppm).

2.4. Powder Characterization. All X-ray diffraction (XRD) patterns shown in Figure 3a were measured at the Pohang Accelerator Laboratory (PAL, 5D XRS GIST beamline). First, sodium-doped triphenylene powder samples were ground finely to add into the capillary tubes (purchased from CTS, Quartz Glass Capillary Tubes 1.0, outer diameter 1.0 mm, length 80 mm, wall thickness 0.01 mm). To maintain inert conditions, the other end was sealed by a torr seal. The X-ray diffraction pattern was obtained in the 2θ range from 5 to 40°. The beam exposure times of pristine triphenylene and sodium-doped triphenylene were 1 and 4 s, respectively. The scan step was 0.02° for both samples, and powder indexing was done by Materials Studio using the DICVOL 91 program in the Reflex module. X-ray diffraction patterns for only ground samples were measured by an in-house machine (Rigaku D/Max 2500 with 40 kV, 100 mA). The powder was placed on the SiO₂ substrate covered using a Kapton film and sealed by Kapton tape.

2.5. Raman Spectroscopy Measurement. Raman scattering measurement was carried out with a Raman spectroscope (Witec) equipped with a 633 nm laser (Research Electro-Optics, Inc.). Capillary samples were prepared using the same methods as for the X-ray diffraction experiment. The laser power was fixed at 0.32 μ W to prevent the burning of sodium-doped triphenylene powder crystals.

2.6. Structure Optimization and Electronic Structure Calculation. In the structure relaxation using the Vienna *ab initio* simulation package (VASP),^{10–12} we optimized the cell using the GGA-PBE¹³ and vdW-DF/revPBE¹⁴ functional. We used $6 \times 2 \times 2$ k points inside the first Brillouin zone and an energy difference cut-off of 1×10^{-5} eV for both ionic relaxation and electronic relaxation.

To calculate the electron–phonon coupling (EPC) of sodium-doped triphenylene, we performed electron–phonon coupling calculations of sodium-doped triphenylene to estimate superconductivity based on the density-functional perturbation theory¹⁵ using Quantum Espresso software.¹⁶ EPC matrix elements were placed in the first Brillouin zone on the $1 \times 1 \times 1$ mesh with the Gamma point mesh for electronic states with a plane-wave basis set cut-off of 100 Ry.

T_c was estimated using the Allen–Dynes equation¹⁷

$$T_c = \frac{\Omega_{\log}}{1.2} \exp\left(-\frac{1.04(1 + \lambda)}{\lambda - \mu^*(1 + 0.62\lambda)}\right)$$

where μ^* is the effective Coulomb interaction parameter, and the normalized weighting function of Eliashberg theory¹⁸ is

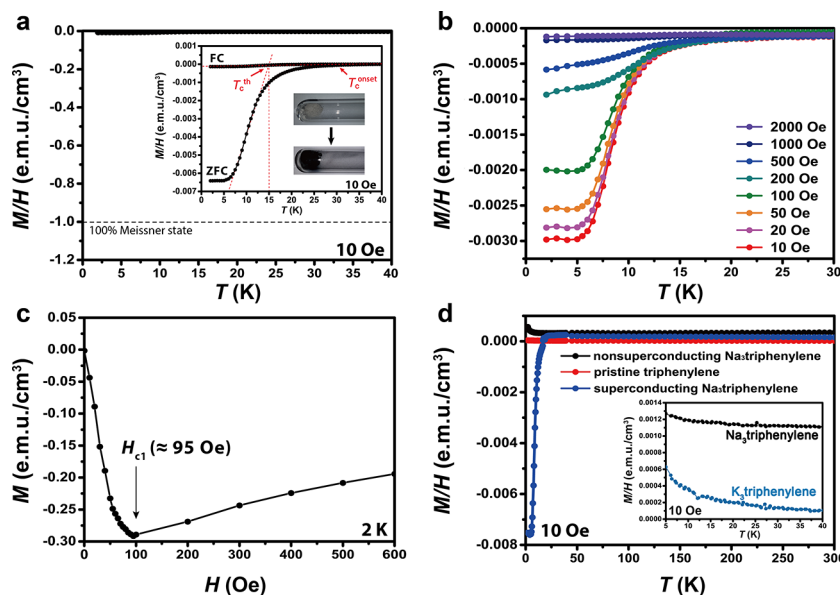


Figure 2. Magnetization measurement for $\text{Na}_3\text{triphenylene}$. (a) M/H versus T curve for ZFC measurement of $\text{Na}_3\text{triphenylene}$ under 10 Oe showing a perfect Meissner state. The inset emphasizes magnetic susceptibility and shows the appearance of ground triphenylene powder with sodium (up) and after annealing (bottom). (b) M/H versus T curves for the ZFC measurement of $\text{Na}_3\text{triphenylene}$ under different magnetic fields. (c) Field-dependent magnetization of $\text{Na}_3\text{triphenylene}$ measured at 2 K. (d) ZFC curves for M/H versus T in the full-temperature region under 10 Oe. Pristine triphenylene powder (red), nonsuperconducting $\text{Na}_3\text{triphenylene}$ powder (black), and superconducting $\text{Na}_3\text{triphenylene}$ (blue), respectively. (Inset) M/H versus T curve for $\text{K}_3\text{triphenylene}$ (sky blue) and nonsuperconducting $\text{Na}_3\text{triphenylene}$ (black) in the region below 40 K.

$$g(\omega) = \frac{2}{\lambda\omega} \alpha^2 F(\omega)$$

λ is the integrated measure of the strength of spectral function $\alpha^2 F$

$$\lambda = 2 \int_0^\infty d\omega \alpha^2 F(\omega) / \omega$$

and the logarithmic average frequency, Ω_{\log} is

$$\Omega_{\log} = \exp \left(\int_0^\infty g(\omega) \ln \omega d\omega \right)$$

3. RESULTS AND DISCUSSION

3.1. Search for Candidate Molecules of PAH Superconductors. To search for candidate molecules of PAH superconductors, we first collected the molecular structure of 200 PAH molecules from the Cambridge Structural Database (CSD)¹⁹ and PubChem.²⁰ The distribution of 200 PAH molecules with respect to their molecular sizes is shown in the Supporting Information (Figure S3). They have various molecular sizes and geometrical shapes. After their molecular structures were optimized using Gaussian 09²¹ with B3LYP^{22,23} exchange–correlation functional and 6-31G(d,p) basis, their molecular energy differences, Δ , were obtained.

In Figure 1a, the distribution of Δ as a function of the number of carbon atoms is shown, and there is no distinct correlation between Δ and the size of the molecules. The reported PAH superconductors, phenanthrene,⁹ picene,⁸ and coronene,²⁴ are marked as circles. Since $\Delta \sim 0.2$ eV is the largest value among those for the reported PAH superconductors so far, we filtered 34 molecules (see the Supporting Information, Table S1) with Δ smaller than 0.2 eV. (1,2:8,9-dibenzo pentacene²⁵ has a larger Δ but a small energy gap between LUMO + 1 and LUMO + 2 levels, which is explained in detail in the Supporting Information, including the case of *p*-terphenyl.²⁶) The filtered molecules were again categorized according to the reported stacking types of the crystals, as

shown in Figure 1b. The stacking types of herringbone, γ -type, and β -type are indicated with circles, diamonds, and squares, respectively. Previously reported superconductors, indicated with filled symbols, have a stacking type of herringbone or γ -type, which is also similar to β -type. PAH molecules with unknown stacking type are indicated by a cross. Candidate PAH molecules with small Δ and a similar stacking type to those for the reported superconductors are listed in Figure 1c. Among the final 10 candidates, phenanthrene (1), picene (2), and coronene (8) are the experimentally reported superconductors, and benzene (7) was theoretically predicted to be a superconductor under high pressure.²⁷ Note that triphenylene (3) was confirmed to be a superconductor by doping sodium in this work.

3.2. Magnetic Susceptibility of $\text{Na}_3\text{triphenylene}$. Sodium-doped triphenylene was prepared via annealing after direct powder grinding of triphenylene with sodium. Figure 2 shows the overall diamagnetic properties of $\text{Na}_3\text{triphenylene}$. The field-cooling (FC) and zero-field-cooling (ZFC) measurements of $\text{Na}_3\text{triphenylene}$ as a function of temperature under 10 Oe are depicted in Figure 2a. In the ZFC curve, a conspicuous decrease of M/H versus T occurred below 15 K, which was the same as from the FC measurement, which means the shielding effect against the applied magnetic field and the corresponding shielding fraction can be estimated to be about 0.65% (assuming the density of $\text{Na}_3\text{triphenylene}$ to be 1.302 g/cm³). This shows that the Meissner effect is manifested in the $\text{Na}_3\text{triphenylene}$ sample, which is the key evidence of superconductivity. The small shielding fraction seems to be caused by the smaller grain size of crystals than the penetration depth of the magnetic field (H) as discussed by Mitsuhashi *et al.*⁸ The M/H curve from $\text{Na}_3\text{triphenylene}$ shown in Figure 2a has moderate transition behavior with an onset temperature of $T_c^{\text{onset}} \approx 30$ K and a critical temperature of $T_c^{\text{th}} = 15$ K, as indicated in Figure 2a. In the last step of the experiment, the superconductivity through the consecutive

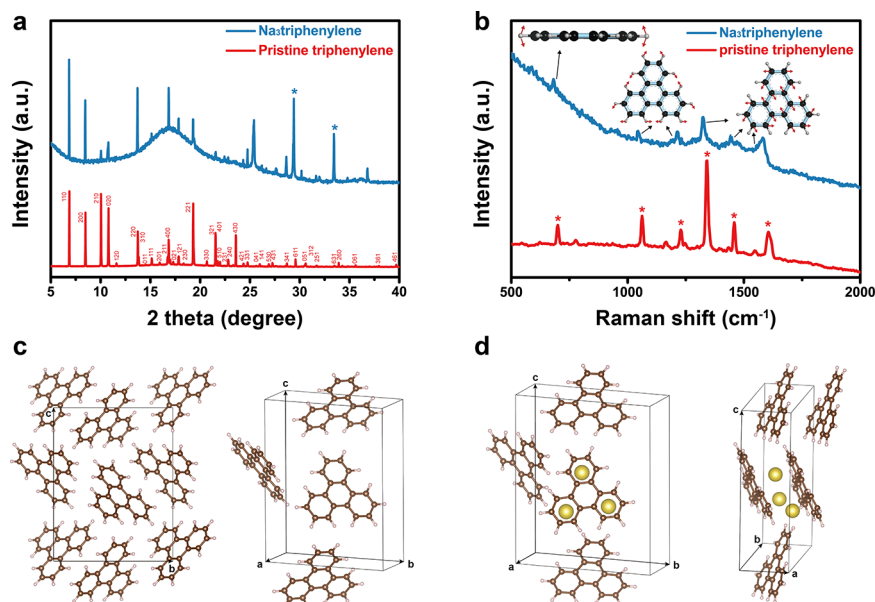


Figure 3. X-ray diffraction patterns and Raman scattering spectra of pristine (red) and superconducting Na_3 triphenylene (sky blue), including the calculated crystal structures. X-ray diffraction patterns and Raman scattering spectra of pristine (red) and superconducting Na_3 triphenylene (sky blue), including calculated crystal structures. (a) X-ray diffraction patterns measured at room temperature under ambient pressure using a capillary. (NaH-related peaks are marked with an asterisk.) (b) Raman scattering spectra measured in the same conditions with XRD measurement. Asterisks indicate the major peaks of pristine triphenylene. These specific vibrational modes are illustrated in (b). The crystal structure of (c) pristine triphenylene and (d) Na_3 triphenylene obtained from *ab initio* calculation. (We indicate only a few molecules in the second and third figure for the sake of easy understanding.)

rapid ZFC measurements was confirmed in 3 of 10 samples made under optimized conditions for the reproducibility test, as shown in the Supporting Information, Figure S4. The magnetic field (H) dependence of M/H versus T shows the drastic suppression of diamagnetic properties above 100 Oe, as shown in Figure 2b. Although the superconducting phase of the powder is gradually destroyed above 100 Oe, the decrease of M/H showing the superconductivity is still observed up to 2000 Oe. One interesting thing to note is that only the shielding fraction seems to be affected by the applied magnetic field. Upon several attempts of heat capacity measurements, no distinct thermodynamic evidence was observed, which appears to be due to the low shielding fraction (see the Supporting Information, Figure S5). In Figure 2c, the lower critical field (H_{c1}) of Na_3 triphenylene is estimated to be about 95 Oe, which is less than those of $\text{K}_{3.33}$ picene ($H_{c1} \approx 380$ Oe, $T_c \approx 18$ K)⁸ and K_3 phenanthrene ($H_{c1} \approx 175$ Oe, $T_c \approx 4.95$ K).⁹ Na_3 triphenylene shows type-II characteristics clearly, like other reported PAH superconductors. Figure 2d shows the magnetic susceptibility of (non-)superconducting sodium-doped triphenylene and pristine triphenylene in a wide range of temperature from 2 to 300 K. While certain $\text{K}_{3.45}$ dibenzopentacenes are reported to have several T_c values,²⁵ the superconducting Na_3 triphenylene in this work has a single T_c value of 15 K. In addition, the pristine triphenylene has a negligible magnetic response unlike the paramagnetic or diamagnetic sodium-doped triphenylene samples. The inset of Figure 2d shows the magnetic susceptibility of potassium-doped triphenylene and non-superconducting sodium-doped triphenylene (nominal composition of K_3 triphenylene and Na_3 triphenylene). K_3 triphenylene shows clear Curie behavior of magnetic susceptibility, which implies that the system has local spin moments with possible Mott insulator behavior.⁷ On the other

hand, the nonsuperconducting Na_3 triphenylene shows almost constant Pauli behavior of magnetic susceptibility and this system is believed to remain metallic. This difference suggests that the size of the alkali metal atom would play an important role in producing the superconductivity in alkali metal-doped PAHs because smaller sodium atoms will result in a metallic state with broad bandwidths of conducting orbitals.

3.3. Crystal Structure and Raman Scattering Spectra of Na_3 triphenylene. The crystal structures of pristine triphenylene and Na_3 triphenylene were measured and analyzed using X-ray diffraction (XRD) and Raman spectroscopy (Figure 3). Each powder sample was filled in the capillary for XRD and Raman measurements. The lattice constants of pristine triphenylene are estimated to be $a = 13.1964$, $b = 16.7912$, and $c = 5.2859$ Å with $\beta = 90^\circ$, which is similar to the reported orthorhombic crystal structure with a space group of $P2_12_12_1$.²⁸

In superconducting Na_3 triphenylene, the main XRD peaks remained to have lattice parameters of $a = 13.1901$, $b = 16.7708$, $c = 5.2760$ Å, and $\beta = 90^\circ$. Negligible change of volume by sodium doping is consistent with the case of K_3 phenanthrene.⁹ Unfortunately, we observed NaH-related peaks in the range of $29\text{--}35^\circ$ (marked with asterisks) like other PAH superconductors,^{9,29} which are believed to be caused by the decomposition of some triphenylene molecules during the mixing or annealing in a vacuum with thermal treatment. However, the other peaks related to the pristine triphenylene still remained. Figure 3b shows the Raman spectra of Na_3 triphenylene and pristine triphenylene. In pristine triphenylene, the main peaks at 1607.26 , 1458.17 , and 1340.98 cm^{-1} are attributed to the stretching of aromatic C–C bonds, those at 1229.02 and 1062.45 cm^{-1} to the in-plane bending of C–H bonds, and that at 699.85 cm^{-1} to the out-of-plane bending of C–H bonds, as listed in Table 1.

Table 1. Major Raman Peak Position of Pristine Triphenylene and Na₃triphenylene

pristine triphenylene (cm ⁻¹)	Na ₃ triphenylene (cm ⁻¹)	assignments
699.85	681.40	C–H out-of-plane bending
1062.45	1044.51	C–H in-plane bending
1229.02	1214.78	C–H in-plane bending
1340.98	1324.88	aromatic C–C stretching
1458.17	1444.42	aromatic C–C stretching
1607.26	1580.59	aromatic C–C stretching

Na₃triphenylene shows conspicuous downshift of the peaks, which indicates the charge transfer to triphenylene from sodium atoms. The peaks from C–C stretching are 1580.59, 1444.42, and 1324.88 cm⁻¹, those from C–H in-plane bending are 1214.78 and 1044.51 cm⁻¹, and that from C–H out-of-plane bending is 681.40 cm⁻¹. Because three sodium atoms are doped to one triphenylene molecule, 5–6 cm⁻¹ of redshift is estimated for one sodium atom.³⁰ A similar size of redshifts has also been observed in M₃C₆₀ (M = K, Rb)^{31,32} and potassium-doped phenanthrene.⁹ The reason for the broadening of peaks in Raman spectra seems to be the formation of amorphous carbon during the annealing process, which would also be another reason for the low shielding fraction.

3.4. Electronic Structures of Na₃triphenylene. We optimized the crystal structure of Na₃triphenylene and calculated its electronic structures using Quantum Espresso¹⁶ and VASP^{10–12} packages. The unit cell contains 4 triphenylene molecules and 12 Na atoms, and its optimized lattice parameters were predicted to be $a = 5.32150$, $b = 14.48530$, and $c = 17.37210$ Å with $\beta = 90^\circ$. Figure 3c,d shows the crystal structures of pristine triphenylene and Na₃triphenylene, respectively. The tilting degree and the position of triphenylene molecules have been slightly changed after the doping of 3 sodium atoms. The optimized positions of the

three sodium atoms are determined to be on the top of each end ring of a triphenylene molecule, which is natural since the end rings are equally more electron-rich than the central ring. The sodium atoms are located between two triphenylene molecules within the ab -plane, which is a result similar to the case of K₃picene⁸ and K₃coronene.²⁴

Based on this optimized crystal structure, we have obtained the electronic structures of Na₃triphenylene. Figure 4a shows the band structure of the conduction bands near the Fermi level. In terms of rigid band theory, Na₃triphenylene has half-filled LUMO + 1 after the doping of three electrons; therefore, the Fermi level has shifted up and become metallic. The band dispersion also indicates the interaction between the triphenylene molecules. Because of the large dispersion along Y–S and X–Γ directions, unlike the b^* and c^* directions, the triphenylene molecules strongly interact along the a^* direction. As mentioned before, in Figure 3d, the molecules are stacked in parallel along the a^* -axis and there are three sodium atoms between them. In terms of the interaction between MOs of aromatic molecules, the three electron-rich end rings of triphenylene molecules are in contact only along the a^* direction. Along the b^* and c^* directions, the electron-pool edges of the molecules are in contact; hence, it shows negligible band dispersion as similarly shown in K₃coronene.²⁴

Figure 4b shows the density of states of Na₃triphenylene. The original band gap of the pristine triphenylene crystal was about 3.1 eV (see the Supporting Information, Figure S6) and Na₃triphenylene has a slightly smaller energy gap below the Fermi level (between the lowest conduction bands and the highest valence bands). Looking at the atom-projected density of states, it is clear that the states at the Fermi level are mainly contributed by carbon atoms, with little contribution from the sodium atoms. In Figure 4c, the isosurfaces of charge density for all integrated k -points for the lowest 4 bands (L) and the next lowest 4 bands (U) of conduction bands are shown. These 8 bands are mainly contributed from the LUMO and LUMO + 1 states of triphenylene molecules. As shown in the

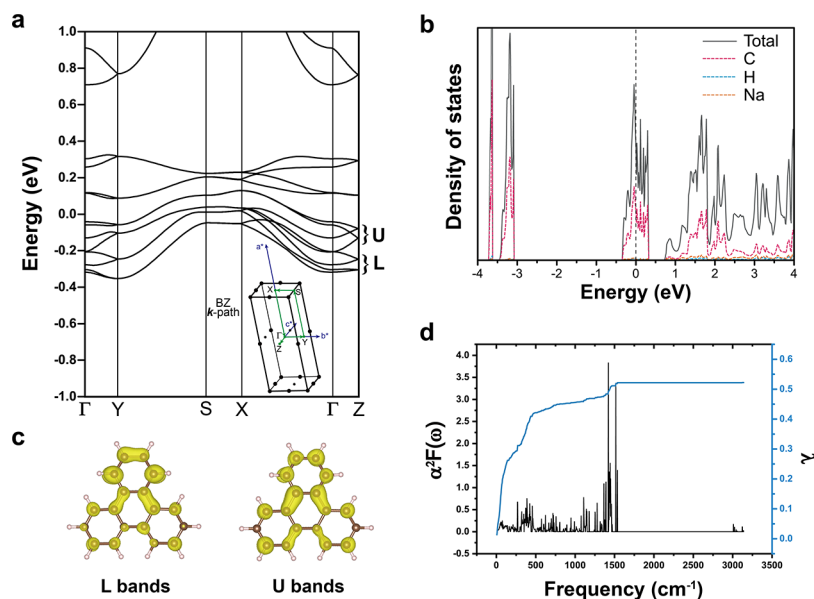


Figure 4. Electronic structure and electron–phonon coupling calculation results of Na₃triphenylene. (a) Band structure and (b) the (top) total and (bottom) atom-projected density of states of Na₃triphenylene. (c) Charge density isosurfaces of (left) the lowest 4 bands (L) and (right) the next lowest 4 bands (U) in (a). (For the sake of brevity, we drew only the charge density for one molecule, not the entire unit cell.) (d) Eliashberg function $\alpha^2F(\omega)$ and the electron–phonon coupling strength λ .

charge density plot, L and U bands evenly have the characteristics of both LUMO and LUMO + 1. It implicitly shows that LUMO and LUMO + 1 are well hybridized and almost degenerate with a very small energy difference of 0.54 meV.

Furthermore, we performed electron–phonon coupling (EPC) calculations to estimate the superconducting transition temperature using the Allen–Dynes equation.¹⁷ Integrated EPC (λ) is predicted to be ~ 0.5 and the corresponding superconducting transition temperature is estimated to be ~ 1.94 K using an effective Coulomb interaction parameter, $\mu^* = 0.13$. The calculated spectral function and the integrated EPC with respect to frequency are shown in Figure 4d, which exhibit frequency-dependent behavior, although there is a quantitative deviation between the calculated and experimentally observed values. We can easily confirm that the lower frequency domain contributed mainly to the coupling, which is the contribution of heavy elements (*i.e.*, sodium). It is worth noting that superconductivity T_c increases with decreasing μ^* ($\mu^* = 0.10$ gives 3.15 K and $\mu^* = 0.03$ gives 6.92 K), which implies that an electron correlation effect at the Fermi level can affect significantly the transition temperature.

4. CONCLUSIONS

In this work, we report the synthesis of a PAH superconductor by doping sodium atoms, which is differentiated from a previous report on the synthesis of PAH superconductors using potassium doping. In the case of C_{60} , which is expected to exhibit superconductivity with sodium doping, the small size of the Na^+ ion causes a disproportionation of Na_3C_{60} into Na_2C_{60} and NaC_{60} due to poor size matching and freezing at the intercalated site.³³ By synthesizing a well-characterized stoichiometry of sodium-doped triphenylene, the superconductivity was first observed in the sodium-doped PAH molecule. Interestingly, all potassium-doped triphenylene samples with the same preparation conditions showed no superconductivity but typical Curie behavior at various doping levels (see the Supporting Information, Figure S7). Therefore, we still have room to increase T_c of alkali metal-doped triphenylene using other alkali metals as a dopant, because T_c is known to rise in proportion to the size of a unit cell.³⁴

Furthermore, superconductivity in sodium-doped triphenylene was found by applying the computational method based on first-principles calculation with the aid of a material database. As mentioned earlier in this paper, it is difficult and takes too much effort to synthesize an alkali metal-doped PAH material and check the superconductivity only with experiments. The veiled mechanism of superconductivity in the PAH material makes it even more difficult to predict new PAH superconductors. Using the computational search method, however, it is possible to judge quickly as to which PAH molecules have a high possibility of exhibiting superconductivity with simple and meaningful physical or empirical parameters. Among the 200 PAH molecules from the database, 34 candidate molecules are suggested to be the possible superconductors with small Δ (see Supporting Information, Table S1). Finally, our computational approach—applying first-principles calculation in the material database to search target materials—is portable to various fields of materials and would help in finding new candidate materials without high costs. Thus, it is worth synthesizing and checking the superconductivity in other candidates consisting of various alkali metal and PAH molecules using our computational

approach, which can help open other pathways to find high- T_c organic superconductors.

■ ASSOCIATED CONTENT

Supporting Information

The Supporting Information is available free of charge at <https://pubs.acs.org/doi/10.1021/acs.chemmater.9b04348>.

X-ray diffraction patterns for ground triphenylene with sodium; real images of color changing of the sample; distribution histogram of PAH molecule data; list of candidate PAH molecules; reproducibility test results; heat capacity and specific heat data; band structure of pristine triphenylene; magnetization of K-doped triphenylene (PDF)

■ AUTHOR INFORMATION

Corresponding Authors

Ji Hoon Shim – Department of Chemistry and Department of Physics, Pohang University of Science and Technology (POSTECH), Pohang 37673, Republic of Korea; orcid.org/0000-0001-7357-0029; Email: jhshim@postech.ac.kr

Hee Cheul Choi – Department of Chemistry, Pohang University of Science and Technology (POSTECH), Pohang 37673, Republic of Korea; orcid.org/0000-0003-1002-1262; Email: choihc@postech.edu

Authors

Taeyung Yoon – Department of Chemistry, Pohang University of Science and Technology (POSTECH), Pohang 37673, Republic of Korea

Ina Park – Department of Chemistry, Pohang University of Science and Technology (POSTECH), Pohang 37673, Republic of Korea; orcid.org/0000-0003-0161-711X

Thao Phuong Nguyen – Department of Chemistry, Pohang University of Science and Technology (POSTECH), Pohang 37673, Republic of Korea; orcid.org/0000-0002-2711-7407

Duck Young Kim – Center for High Pressure Science and Technology Advanced Research (HPSTAR), Shanghai 201203, China; Department of Chemistry, Pohang University of Science and Technology (POSTECH), Pohang 37673, Republic of Korea

Jinho Lee – Department of Chemistry, Pohang University of Science and Technology (POSTECH), Pohang 37673, Republic of Korea

Complete contact information is available at: <https://pubs.acs.org/doi/10.1021/acs.chemmater.9b04348>

Author Contributions

^{||}T.Y. and I.P. contributed equally to this work.

Notes

The authors declare no competing financial interest.

■ ACKNOWLEDGMENTS

The authors thank J. S. Kim for fruitful discussion. The work conducted by J.H.S was supported by the National Research Foundation of Korea (Grant No. 2017R1D1A1B03032069). H.C.C. acknowledges funding from the Veteran Researcher Grant (No. 2019R1A2C2004259) managed by the National Research Foundation of Korea (NRF) and Samsung Electronics. D.Y.K. acknowledges the support by the NSFC

of China (Grant No. 11774015) and the National Research Foundation of Korea (NRF-2020R1A2C1005236).

REFERENCES

- (1) Hannay, N. B.; Geballe, T. H.; Matthias, B. T.; Andres, K.; Schmidt, P.; MacNair, D. Superconductivity in Graphitic Compounds. *Phys. Rev. Lett.* **1965**, *14*, 225–226.
- (2) Tang, Z. K.; Zhang, L.; Wang, N.; Zhang, X. X.; Wen, G. H.; Li, G. D.; Wang, J. N.; Chan, C. T.; Sheng, P. Superconductivity in 4 angstrom single-walled carbon nanotubes. *Science* **2001**, *292*, 2462–2465.
- (3) Kociak, M.; Kasumov, A. Y.; Guéron, S.; Reulet, B.; Khodos, I. I.; Gorbatov, Y. B.; Volkov, V. T.; Vaccarini, L.; Bouchiat, H. Superconductivity in Ropes of Single-Walled Carbon Nanotubes. *Phys. Rev. Lett.* **2001**, *86*, 2416–2419.
- (4) Xue, M.; Chen, G.; Yang, H.; Zhu, Y.; Wang, D.; He, J.; Cao, T. Superconductivity in Potassium-Doped Few-Layer Graphene. *J. Am. Chem. Soc.* **2012**, *134*, 6536–6539.
- (5) Schilling, A.; Cantoni, M.; Guo, J. D.; Ott, H. R. Superconductivity above 130 K in the Hg-Ba-Ca-Cu-O system. *Nature* **1993**, *363*, 56–58.
- (6) Wu, G.; Xie, Y. L.; Chen, H.; Zhong, M.; Liu, R. H.; Shi, B. C.; Li, Q. J.; Wang, X. F.; Wu, T.; Yan, Y. J.; Ying, J. J.; Chen, X. H. Superconductivity at 56 K in samarium-doped SrFeAsF. *J. Phys.: Condens. Matter* **2009**, *21*, No. 142203.
- (7) Kim, M.; Choi, H. C.; Shim, J. H.; Min, B. I. Correlated electronic structures and the phase diagram of hydrocarbon-based superconductors. *New J. Phys.* **2013**, *15*, No. 113030.
- (8) Mitsuhashi, R.; Suzuki, Y.; Yamanari, Y.; Mitamura, H.; Kambe, T.; Ikeda, N.; Okamoto, H.; Fujiwara, A.; Yamaji, M.; Kawasaki, N.; Maniwa, Y.; Kubozono, Y. Superconductivity in alkali-metal-doped picene. *Nature* **2010**, *464*, 76–79.
- (9) Wang, X. F.; Liu, R. H.; Gui, Z.; Xie, Y. L.; Yan, Y. J.; Ying, J. J.; Luo, X. G.; Chen, X. H. Superconductivity at 5 K in alkali-metal-doped phenanthrene. *Nat. Commun.* **2011**, *2*, No. 507.
- (10) Kresse, G.; Hafner, J. *Ab initio* molecular dynamics simulation of the liquid-metal-amorphous-semiconductor transition in germanium. *Phys. Rev. B* **1994**, *49*, 14251.
- (11) Kresse, G.; Furthmüller, J. Efficiency of *ab-initio* total energy calculations for metals and semiconductors using a plane-wave basis set. *Comput. Mater. Sci.* **1996**, *6*, 15–50.
- (12) Kresse, G.; Furthmüller, J. Efficient iterative schemes for *ab initio* total-energy calculations using a plane-wave basis set. *Phys. Rev. B* **1996**, *54*, 11169.
- (13) Perdew, J. P.; Burke, K.; Ernzerhof, M. Generalized gradient approximation made simple. *Phys. Rev. Lett.* **1996**, *77*, 3865–3868.
- (14) Dion, M.; Rydberg, H.; Schröder, E.; Langreth, D. C.; Lundqvist, B. I. Van der Waals density functional for general geometries. *Phys. Rev. Lett.* **2004**, *92*, No. 246401.
- (15) Baroni, S.; de Gironcoli, S.; Corso, D. A.; Giannozzi, P. Phonons and related crystal properties from density-functional perturbation theory. *Rev. Mod. Phys.* **2001**, *73*, 515–562.
- (16) Giannozzi, P.; Baroni, S.; Bonini, N.; Calandra, M.; Car, R.; Cavazzoni, C.; Ceresoli, D.; Chiarotti, G. L.; Cococcioni, M.; Dabo, I.; Corso, A. D.; de Gironcoli, S.; Fabris, S.; Fratesi, G.; Gebauer, R.; Gerstmann, U.; Gougoussis, C.; Kokalj, A.; Lazzeri, M.; Martin-Samos, L.; Marzari, N.; Mauri, F.; Mazzarello, R.; Paolini, S.; Pasquarello, A.; Paulatto, L.; Sbraccia, C.; Scandolo, S.; Sclauzero, G.; Seitsonen, A.; Smogunov, A.; Umari, P.; Wentzcovitch, R. M. QUANTUM ESPRESSO: a modular and open-source software project for quantum simulations of materials. *J. Phys.: Condens. Matter* **2009**, *21*, No. 395502.
- (17) Allen, P. B.; Dynes, R. C. Transition temperature of strong-coupled superconductors reanalyzed. *Phys. Rev. B* **1975**, *12*, 905–922.
- (18) McMillan, W. L. Transition Temperature of Strong-Coupled Superconductors. *Phys. Rev.* **1968**, *167*, 331–344.
- (19) Groom, C. R.; Bruno, I. J.; Lightfoot, M. P.; Ward, S. C. The Cambridge Structural Database. *Acta Crystallogr., Sect. B: Struct. Sci., Cryst. Eng. Mater.* **2016**, *72*, 171–179.
- (20) Kim, S.; Chen, J.; Cheng, T.; Gindulyte, A.; He, J.; He, S.; Li, Q.; Shoemaker, B. A.; Thiessen, P. A.; Yu, B.; Zaslavsky, L.; Zhang, J.; Bolton, E. E. PubChem 2019 update: improved access to chemical data. *Nucleic Acids Res.* **2019**, *47*, D1102–D1109.
- (21) Frisch, M. J.; Trucks, G. W.; Schlegel, H. B.; Scuseria, G. E.; Robb, M. A.; Cheeseman, J. R.; Scalmani, G.; Barone, V.; Petersson, G. A.; Nakatsuji, H.; Li, X.; Caricato, M.; Marenich, A.; Bloino, J.; Janesko, B. G.; Gomperts, R.; Mennucci, B.; Hratchian, H. P.; Ortiz, J. V.; Izmaylov, A. F.; Sonnenberg, J. L.; Williams-Young, D.; Ding, F.; Lipparini, F.; Egidi, F.; Goings, J.; Peng, B.; Petrone, A.; Henderson, T.; Ranasinghe, D.; Zakrzewski, V. G.; Gao, J.; Rega, N.; Zheng, G.; Liang, W.; Hada, M.; Ehara, M.; Toyota, K.; Fukuda, R.; Hasegawa, J.; Ishida, M.; Nakajima, T.; Honda, Y.; Kitao, O.; Nakai, H.; Vreven, T.; Throssell, K.; Montgomery, J. A., Jr.; Peralta, J. E., Jr.; Ogliaro, F.; Bearpark, M.; Heyd, J. J.; Brothers, E.; Kudin, K. N.; Staroverov, V. N.; Keith, T.; Kobayashi, R.; Normand, J.; Raghavachari, K.; Rendell, A.; Burant, J. C.; Iyengar, S. S.; Tomasi, J.; Cossi, M.; Millam, J. M.; Klene, M.; Adamo, C.; Cammi, R.; Ochterski, J. W.; Martin, R. L.; Morokuma, K.; Farkas, O.; Foresman, J. B.; Fox, D. J. *Gaussian09*; Gaussian, Inc.: Wallingford CT, 2016.
- (22) Becke, A. D. Density-functional thermochemistry. III. The role of exact exchange. *J. Chem. Phys.* **1993**, *98*, 5648–5652.
- (23) Lee, C.; Yang, W.; Parr, R. G. Development of the Colle-Salvetti correlation-energy formula into a functional of the electron density. *Phys. Rev. B* **1988**, *37*, 785–789.
- (24) Kubozono, Y.; Mitamura, H.; Lee, X.; He, X.; Yamanari, Y.; Takahashi, Y.; Suzuki, Y.; Kaji, Y.; Eguchi, R.; Akaike, K.; Kambe, T.; Okamoto, H.; Fujiwara, A.; Kato, T.; Kosugi, T.; Aoki, H. Metal-intercalated aromatic hydrocarbons: a new class of carbon-based superconductors. *Phys. Chem. Chem. Phys.* **2011**, *13*, 16476–16493.
- (25) Xue, M.; Cao, T.; Wang, D.; Wu, Y.; Yang, H.; Dong, X.; He, J.; Li, F.; Chen, G. F. Superconductivity above 30 K in alkali-metal-doped hydrocarbon. *Sci. Rep.* **2012**, *2*, No. 389.
- (26) Zhong, G.-H.; Wang, X.-H.; Wang, R.-S.; Han, J.-X.; Zhang, C.; Chen, X.-J.; Lin, H.-Q. Structural and Bonding Characteristics of Potassium-Doped *p*-Terphenyl Superconductors. *J. Phys. Chem. C* **2018**, *122*, 3801–3808.
- (27) Zhong, G. H.; Yang, C. L.; Chen, X. J.; Lin, H. Q. Superconductivity in solid benzene molecular crystal. *J. Phys.: Condens. Matter* **2018**, *30*, No. 245703.
- (28) Ahmed, F. R.; Trotter, J. The crystal structure of triphenylene. *Acta Crystallogr.* **1963**, *16*, 503–508.
- (29) Teranishi, K.; He, X.; Sakai, Y.; Izumi, M.; Goto, H.; Eguchi, R.; Takabayashi, Y.; Kambe, T.; Kubozono, Y. Observation of zero resistivity in K-doped picene. *Phys. Rev. B* **2013**, *87*, No. 060505(R).
- (30) Colangeli, L.; Mennella, V.; Baratta, G. A.; Bussoletti, E.; Strazzulla, G. Raman and infrared spectra of polycyclic aromatic hydrocarbon molecules of possible astrophysical interest. *Astrophys. J.* **1992**, *396*, 369–377.
- (31) Zhou, P.; Wang, K.-A.; Rao, A. M.; Eklund, P. C.; Dresselhaus, G.; Dresselhaus, M. S. Raman-scattering studies of homogeneous K₃C₆₀ films. *Phys. Rev. B* **1992**, *45*, No. 10838(R).
- (32) Kelly, M. K.; Thomsen, C. Excitation energy and temperature-dependent Raman study of Rb₃C₆₀ films. *Phys. Rev. B* **1994**, *50*, 18572–18579.
- (33) Rosseinsky, M. J.; Murphy, D. W.; Fleming, R. M.; Tycko, R.; Ramirez, A. P.; Dabbagh, G.; Barrett, S. E. Structural and electronic properties of sodium-intercalated C₆₀. *Nature* **1992**, *356*, 416–418.
- (34) Fleming, R. M.; Ramirez, A. P.; Rosseinsky, M. J.; Murphy, D. W.; Haddon, R. C.; Zahurak, S. M.; Makhija, A. V. Relation of structure and superconducting transition temperature in A₃C₆₀. *Nature* **1991**, *352*, 787–788.